An Implicit Form for the Osher Upwind Scheme

Man Mohan Rai*
NASA Ames Research Center, Moffett Field, California
and
Sukumar R. Chakravarthy†
Rockwell International Science Center, Thousand Oaks, California

Conservative upwind schemes for the Euler equations, such as the Osher scheme, accurately resolve flow discontinuities and correctly model the physics of the problem. However, these schemes require many more arithmetic operations per integration step than simple central-difference schemes and hence, result in large computing times. An implicit version of the first-order- and second-order-accurate Osher schemes in two spatial dimensions and generalized coordinates is developed in this study. Because implicit schemes permit the use of large integration steps, in many cases they require fewer integration steps to reach steady-state (especially in calculations on grids with widely varying mesh-cell sizes). The implicit scheme developed in this study accelerated convergence speeds by almost an order of magnitude in the problems considered. Test cases include quasi-one-dimensional nozzle flow and supersonic flow past a cylinder.

Introduction

WITH the advent of conservative upwind schemes, such as the Osher scheme,[1,2] complex flowfields containing flow discontinuities (e.g., shocks and slip surfaces) can be simulated numerically with minimal effort[3] (as opposed to shock-fitting schemes which require extensive, problem-dependent logic to be built into the program to treat discontinuities). The conservative nature of such schemes permits users to resolve flow discontinuities accurately without having to treat the discontinuities in a special manner (shock and slip surfaces are "captured" automatically). Conservative central-difference schemes can also be used to capture shocks; however, they often require the use of arbitrary smoothing parameters to stabilize the calculation and cannot be relied upon to capture strong shocks, i.e., where the pressure ratio across the shock is greater than 10.0. Upwind schemes, on the other hand, have been used to capture extremely strong shocks and do not require the use of arbitrary parameters. Shocks with pressure ratios of approximately 75.0 have been captured with ease.[2] To capture shocks of this strength with a central-difference scheme would require excessive smoothing, which in turn would degrade the solution considerably. Consequently, central-difference schemes are not as robust as upwind schemes and also do not model the physics of the problem as accurately as upwind schemes.

In general, upwind schemes can be expected to yield results that are superior to those obtained with central-difference schemes (because of the reasons mentioned previously). However, this improvement in the quality of the numerical solution is obtained at the expense of programming simplicity and computational speed. Typically, upwind schemes require many more arithmetic operations per integration step than simple central-difference schemes and, hence, their use results in larger computing times. Therefore, it is advantageous to be able to take integration step sizes larger than those possible with explicit upwind schemes so that the final solution is obtained in fewer integration steps and at lower computational cost (i.e., lower than the cost incurred with an explicit scheme).

The Osher scheme is a robust, conservative, upwind scheme with excellent shock-capturing capability. References 1 and 2 present the first-order- and second-order-accurate explicit Osher schemes. The explicit nature of these schemes restricts the maximum allowable integration step size in the usual way. An implicit form for the first-order- and second-order-accurate versions of the Osher scheme is presented herein. The equations are developed in one and two spatial dimensions (and in generalized coordinates for the two-dimensional case). The convergence rate was increased by about an order of magnitude for most of the problems considered. Test cases include quasi-one-dimensional nozzle flow and supersonic flow past a cylinder.

The Implicit Scheme

The Implicit Scheme in One Spatial Dimension

Consider the unsteady Euler equations in one dimension:

$$Q_t + E_x = 0 \tag{1}$$

The vectors Q and E are given by

$$Q = \begin{bmatrix} \rho \\ \rho u \\ e \end{bmatrix}, \quad E = \begin{bmatrix} \rho u \\ p + \rho u^2 \\ (e+p)u \end{bmatrix} \tag{2}$$

where ρ is the density, p the pressure, u the velocity in the x direction, and e the total internal energy per unit volume,

$$e = \frac{p}{\gamma - 1} + \frac{\rho u^2}{2} \tag{3}$$

A conservative finite difference scheme for Eq. (1) can be written as

$$\frac{Q_i^{n+1} - Q_i^n}{\Delta t} + \frac{\hat{E}_{i+1/2}^m - \hat{E}_{i-1/2}^m}{\Delta x} = 0 \tag{4}$$

Received Dec. 12, 1983; presented as Paper 84-0088 at AIAA 22nd Aerospace Sciences Meeting, Reno, NV, Jan. 9-12, 1984; revision received Aug. 2, 1985. This paper is declared a work of the U.S. Government and is not subject to copyright protection in the United States.

*Principal Analyst, Informatics General Corporation. Member AIAA.
†Research Scientist. Member AIAA.

where $\hat{E}^m_{i+1/2}$ is the numerical flux consistent with the physical flux E. The difference scheme [Eq. (4)] is explicit when $m=n$ and fully implicit when $m=n+1$.

The numerical flux for the first-order-accurate Osher scheme[1] is given by

$$\hat{E}_{i+1/2}=\frac{1}{2}\left[E_i+E_{i+1}-\int_{Q_i}^{Q_{i+1}}\left\{\left\{\frac{\partial E}{\partial Q}\right\}^+-\left\{\frac{\partial E}{\partial Q}\right\}^-\right\}dQ\right] \quad (5)$$

To evaluate the integral in Eq. (5), two intermediate points are introduced between the points i and $i+1$. They are denoted as points $i+1/3$ and $i+2/3$, as shown in Fig. 1. These intermediate points lie in phase space and define three subpaths along which the integral is evaluated. Each subpath is associated with a particular eigenvalue of the Jacobian matrix $\partial E/\partial Q$ and a set of Riemann invariants. The Riemann invariants of a given subpath remain constant along the subpath. This property is utilized in calculating the dependent variables and fluxes at the points $i+1/3$ and $i+2/3$.

The values of the dependent variables at the intermediate points are obtained from the following equations:

$$\begin{aligned}
&u_{i+1/3}+\frac{2}{\gamma-1}c_{i+1/3}=u_i+\frac{2}{\gamma-1}c_i\\
&\frac{p_{i+1/3}}{\rho^\gamma_{i+1/3}}=\frac{p_i}{\rho^\gamma_i},\\
&p_{i+2/3}=p_{i+1/3}\\
&u_{i+2/3}=u_{i+1/3}\\
&u_{i+2/3}-\frac{2}{\gamma-1}c_{i+2/3}=u_{i+1}-\frac{2}{\gamma-1}c_{i+1}\\
&\frac{p_{i+2/3}}{\rho^\gamma_{i+2/3}}=\frac{p_{i+1}}{\rho^\gamma_{i+1}}
\end{aligned} \quad (6)$$

where

$$c=(\gamma p/\rho)^{1/2}$$

Equations (6) constitute a system of six equations and can be solved to yield the six dependent variables ($\rho_{i+1/3}$, $u_{i+1/3}$, $p_{i+1/3}$, $\rho_{i+2/3}$, $u_{i+2/3}$, $p_{i+2/3}$) at the intermediate points. The relationship between the dependent variables at the intermediate points in phase space and the dependent variables Q_i and Q_{i+1} can also be expressed as

$$\begin{aligned}
Q_{i+1/3}&=Q_{i+1/3}(Q_i,Q_{i+1})\\
Q_{i+2/3}&=Q_{i+2/3}(Q_i,Q_{i+1})
\end{aligned} \quad (7)$$

The exact functional forms of the relationships in Eqs. (7) can be found in Refs. 1 and 2.

Denoting the eigenvalues corresponding to the three subpaths (i, $i+1/3$), ($i+1/3$, $i+2/3$), and ($i+2/3$, $i+1$) as $\lambda^{(1)}$, $\lambda^{(2)}$, and $\lambda^{(3)}$, we have

$$\lambda^{(1)}=u-c, \quad \lambda^{(2)}=u, \quad \lambda^{(3)}=u+c \quad (8)$$

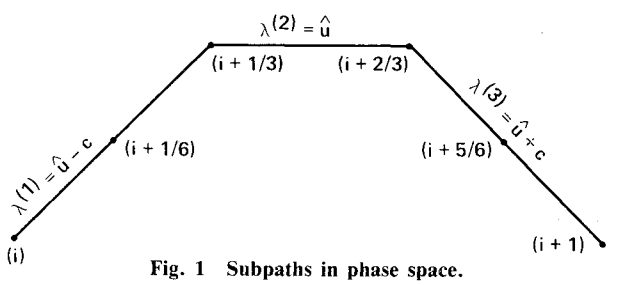

Fig. 1 Subpaths in phase space.

Also, let

$$\begin{aligned}
\Delta E^+&=\int_{Q_i}^{Q_{i+1}}\left\{\frac{\partial E}{\partial Q}\right\}^+dQ\\
\Delta E^-&=\int_{Q_i}^{Q_{i+1}}\left\{\frac{\partial E}{\partial Q}\right\}^-dQ
\end{aligned} \quad (9)$$

Then, ΔE^+ can be written as

$$\Delta E^+=(\Delta E^+)^{(1)}+(\Delta E^+)^{(2)}+(\Delta E^+)^{(3)} \quad (10)$$

where

$$\begin{aligned}
(\Delta E^+)^{(1)}&=k_{i,i+1/3}(E_{i+1/3}-E_i)\\
(\Delta E^+)^{(2)}&=k_{i+1/3,i+2/3}(E_{i+2/3}-E_{i+1/3})\\
(\Delta E^+)^{(3)}&=k_{i+2/3,i+1}(E_{i+1}-E_{i+2/3})\\
k_{i+(j-1)/3,i+j/3}&=1, \quad \text{if } \lambda^{(j)}_{i+(j-1)/3},\lambda^{(j)}_{i+j/3}\geq 0\\
&=0, \quad \text{if } \lambda^{(j)}_{i+(j-1)/3},\lambda^{(j)}_{i+j/3}<0\\
&\qquad j=1,2,3
\end{aligned} \quad (11)$$

Similarly, ΔE^- can be written as

$$\Delta E^-=(\Delta E^-)^{(1)}+(\Delta E^-)^{(2)}+(\Delta E^-)^{(3)} \quad (12)$$

where

$$\begin{aligned}
(\Delta E^-)^{(1)}&=\ell_{i,i+1/3}(E_{i+1/3}-E_i)\\
(\Delta E^-)^{(2)}&=\ell_{i+1/3,i+2/3}(E_{i+2/3}-E_{i+1/3})\\
(\Delta E^-)^{(3)}&=\ell_{i+2/3,i+1}(E_{i+1}-E_{i+2/3})\\
\ell_{i+(j-1)/3,i+j/3}&=1-k_{i+(j-1)/3,i+j/3}, \quad j=1,2,3
\end{aligned} \quad (13)$$

Equations (11) and (13) do not account for the cases in which the eigenvalue changes sign within a given subpath. Consider the case in which $\lambda^{(1)}$ changes sign along the subpath $(i,i+1/3)$. Let the point denoted as $i+1/6$ in Fig. 1 represent the point in phase space at which $\lambda^{(1)}$ is equal to zero. Then, the following relationship is true at $i+1/6$:

$$u_{i+1/6}-c_{i+1/6}=0 \quad (14)$$

The dependent variables at point $i+1/6$ can be easily determined from Eqs. (6) and (14). The expression for $(\Delta E^+)^{(1)}$ now becomes

$$(\Delta E^+)^{(1)}=k_{i,i+1/6}[E_{i+1/6}-E_i]+k_{i+1/6,i+1/3}[E_{i+1/3}-E_{i+1/6}] \quad (15)$$

where

$$\begin{aligned}
k_{i+(j-1)/6,i+j/6}&=1, \quad \text{if } \lambda^{(1)}_{i+(j-1)/6},\lambda^{(1)}_{i+j/6}\geq 0\\
&=0, \quad \text{if } \lambda^{(1)}_{i+(j-1)/6},\lambda^{(1)}_{i+j/6}<0 \quad j=1,2
\end{aligned} \quad (16)$$

and $(\Delta E^-)^{(1)}$ can be written as

$$(\Delta E^-)^{(1)}=\ell_{i,i+1/6}[E_{i+1/6}-E_i]+\ell_{i+1/6,i+1/3}[E_{i+1/3}-E_{i+1/6}] \quad (17)$$

where

$$\ell_{i,i+1/6}=1-k_{i,i+1/6}$$

$$\ell_{i+1/6,i+1/3}=1-k_{i+1/6,i+1/3} \quad (18)$$

The treatment of the case in which $\lambda^{(3)}$ changes sign in the subpath $(i+2/3, i+1)$ is very similar. Further details of the explicit, first-order-accurate Osher scheme can be found in Refs. 1 and 2.

For a fully implicit scheme, it is required that the fluxes be evaluated at the $(n+1)$th time level. However, evaluation of the fluxes at the $(n+1)$th time level results in a system of nonlinear equations that, in general, needs to be solved in an iterative manner. To develop a set of linear implicit equations that can be solved in a noniterative fashion, it is necessary to linearize the numerical fluxes with respect to time (t). The resulting set of equations is a linearized form of the fully implicit scheme. The numerical flux $\hat{E}^{n+1}_{i+1/2}$ can be written, using Eqs. (5) and (9), as

$$\hat{E}^{n+1}_{i+1/2} = 1/2[E^{n+1}_i + E^{n+1}_{i+1} - (\Delta E^+)^{n+1} + (\Delta E^-)^{n+1}] \quad (19)$$

Consider the linearization of $(\Delta E^+)^{n+1}$:

$$\begin{aligned}(\Delta E^+)^{n+1} = (\Delta E^+)^n &+ k^n_{i,i+1/3}\left\{\left\{\frac{\partial E}{\partial Q}\right\}^n_{i+1/3}\Delta Q_{i+1/3} - \left\{\frac{\partial E}{\partial Q}\right\}_i \Delta Q_i\right\} + k^n_{i+1/3,i+2/3}\left\{\left\{\frac{\partial E}{\partial Q}\right\}^n_{i+2/3}\Delta Q_{i+2/3} - \left\{\frac{\partial E}{\partial Q}\right\}^n_{i+1/3}\Delta Q_{i+1/3}\right\} \\ &+ k^n_{i+2/3,i+1}\left\{\left\{\frac{\partial E}{\partial Q}\right\}^n_{i+1}\Delta Q_{i+1} - \left\{\frac{\partial E}{\partial Q}\right\}^n_{i+2/3}\Delta Q_{i+2/3}\right\} \end{aligned} \quad (20)$$

For the sake of simplicity, the cases in which the eigenvalues change sign within their associated subpaths have not been included in Eq. (20). However, the linearization procedure is similar even under such conditions. The terms $\Delta Q_{i+1/3}$ and $\Delta Q_{i+2/3}$ can be related to ΔQ_i and ΔQ_{i+1}. This relationship is established by differentiating Eqs. (7). The resulting equations can be written as

$$\begin{aligned}\Delta Q_{i+1/3} &= M^n_{i+1/3,i}\Delta Q_i + M^n_{i+1/3,i+1}\Delta Q_{i+1} \\ \Delta Q_{i+2/3} &= M^n_{i+2/3,i}\Delta Q_i + M^n_{i+2/3,i+1}\Delta Q_{i+1}\end{aligned} \quad (21)$$

where $M^n_{i+1/3,i}$, $M^n_{i+1/3,i+1}$, $M^n_{i+2/3,i}$, and $M^n_{i+2/3,i+1}$ are Jacobian matrices obtained from differentiating Eqs. (7) and are given by

$$M^n_{i+1/3,i} = \left(\frac{\partial Q_{i+1/3}}{\partial Q_i}\right)^n \qquad M^n_{i+1/3,i+1} = \left(\frac{\partial Q_{i+1/3}}{\partial Q_{i+1}}\right)^n$$

$$M^n_{i+2/3,i} = \left(\frac{\partial Q_{i+2/3}}{\partial Q_i}\right)^n \qquad M^n_{i+2/3,i+1} = \left(\frac{\partial Q_{i+2/3}}{\partial Q_{i+1}}\right)^n$$

A different method of obtaining the Jacobian matrices is given in Ref. 4. Substituting Eqs. (21) into Eq. (20) gives

$$\begin{aligned}(\Delta E^+)^{n+1} = (\Delta E^+)^n &+ \left\{k^n_{i,i+1/3}\left\{\left\{\frac{\partial E}{\partial Q}\right\}^n_{i+1/3}M^n_{i+1/3,i} - \left\{\frac{\partial E}{\partial Q}\right\}^n_i\right\} + k^n_{i+1/3,i+2/3}\left\{\left\{\frac{\partial E}{\partial Q}\right\}^n_{i+2/3}M^n_{i+2/3,i} - \left\{\frac{\partial E}{\partial Q}\right\}^n_{i+1/3}M^n_{i+1/3,i}\right\} - k^n_{i+2/3,i+1}\left\{\frac{\partial E}{\partial Q}\right\}^n_{i+2/3}M^n_{i+2/3,i}\right\}\Delta Q_i \\ &+ \left\{k^n_{i,i+1/3}\left\{\frac{\partial E}{\partial Q}\right\}^n_{i+1/3}M^n_{i+1/3,i+1} + k^n_{i+1/3,i+2/3}\left\{\left\{\frac{\partial E}{\partial Q}\right\}^n_{i+2/3}M^n_{i+2/3,i+1} - \left\{\frac{\partial E}{\partial Q}\right\}^n_{i+1/3}M^n_{i+1/3,i+1}\right\} + k^n_{i+2/3,i+1}\right. \\ &\left.\times\left\{\left\{\frac{\partial E}{\partial Q}\right\}^n_{i+1} - \left\{\frac{\partial E}{\partial Q}\right\}^n_{i+2/3}M^n_{i+2/3,i+1}\right\}\right\}\Delta Q_{i+1}\end{aligned} \quad (22)$$

A similar linearization of $(\Delta E^-)^{n+1}$ is required to linearize the numerical flux $\hat{E}^{n+1}_{i+1/2}$. It is clear from Eq. (22) that the linearization of the numerical flux associated with the Osher scheme is a tedious procedure and will require a great number of arithmetic operations.

An extremely simply linearization is obtained if the following approximation is made:

$$\left(\frac{\partial E}{\partial Q}\right)^+ \simeq \frac{\partial (E^+)}{\partial Q}$$

$$\left(\frac{\partial E}{\partial Q}\right)^- \simeq \frac{\partial (E^-)}{\partial Q} \quad (23)$$

The justification for this approximation can be found in Ref. 5, although in a different context. Substitution of Eqs. (23) into Eq. (5) yields

$$\hat{E}_{i+1/2} = E^+_i + E^-_{i+1} \quad (24)$$

Note that Eq. (24) defines the numerical flux for the first-order-accurate split-flux scheme of Steger and Warming.[5] Linearization of Eq. (24) yields

$$\hat{E}^{n+1}_{i+1/2} = \hat{E}^n_{i+1/2} + \left\{\frac{\partial (E^+)}{\partial Q}\right\}_i \Delta Q_i + \left\{\frac{\partial (E^-)}{\partial Q}\right\}_{i+1}\Delta Q_{i+1} \quad (25)$$

Substituting Eqs. (23) into Eq. (25) results in the following linearization of the numerical flux:

$$\hat{E}^{n+1}_{i+1/2} = \hat{E}^n_{i+1/2} + A^+_i\Delta Q_i + A^-_{i+1}\Delta Q_{i+1} \quad (26)$$

where

$$A^+ = \left\{\frac{\partial E}{\partial Q}\right\}^+, \quad A^- = \left\{\frac{\partial E}{\partial Q}\right\}^- \quad (27)$$

The approximate linearization introduced in Eqs. (23) has been found to result in an upper limit on Δt for stability in calculations with the split-flux scheme.[6] However, in two and three dimensions, the stability limit imposed by approximate factorization can be much more restrictive than that imposed by Eqs. (23).

The implicit method obtained using the preceding linearization [Eq. (26)] can now be written as

$$\left[I + \frac{\Delta t}{\Delta x}(\Delta_x A^- + \nabla_x A^+)\right]^n \Delta Q_i = -\frac{\Delta t}{\Delta x}(\hat{E}^n_{i+1/2} - \hat{E}^n_{i-1/2}) \quad (28)$$

where Δ and ∇ are forward and backward difference operators, respectively. Note that the numerical flux $\hat{E}^n_{i+1/2}$ used in Eq. (28) is obtained from Eq. (5) and not from Eq. (24); i.e., the left-hand side of Eq. (28) corresponds to the split-flux scheme and the right-hand side of Eq. (28) corresponds to the Osher scheme.

The Implicit Scheme in Two Spatial Dimensions

Consider the unsteady Euler equations in two dimensions:

$$Q_t + E_x + F_y = 0 \quad (29)$$

The vectors Q, E, and F are given by

$$Q = \begin{bmatrix}\rho \\ \rho u \\ \rho v \\ e\end{bmatrix}, \quad E = \begin{bmatrix}\rho u \\ p + \rho u^2 \\ \rho uv \\ (e+p)u\end{bmatrix}, \quad F = \begin{bmatrix}\rho v \\ \rho uv \\ p + \rho v^2 \\ (e+p)v\end{bmatrix} \quad (30)$$

where ρ is the density, p the pressure, u and v the velocities in the x and y directions, respectively, and e the total energy per unit volume,

$$e=\frac{p}{\gamma-1}+\frac{\rho}{2}(u^2+v^2) \tag{31}$$

Under the independent variable transformation

$$\tau=t, \quad \xi=\xi(x,y,t), \quad \eta=\eta(x,y,t) \tag{32}$$

Equation (29) transforms into

$$\tilde{Q}_\tau+\tilde{E}_\xi+\tilde{F}_\eta=0 \tag{33}$$

where

$$Q=Q/J$$

$$\tilde{E}(Q,\xi)=(\xi_t Q+\xi_x E+\xi_y F)/J$$

$$\tilde{F}(Q,\eta)=(\eta_t Q+\eta_x E+\eta_y F)/J$$

$$J=\xi_x\eta_y-\eta_x\xi_y \tag{34}$$

The notation $\tilde{E}(Q,\xi)$ and $\tilde{F}(Q,\eta)$ is used to show the dependence of these quantities on the metrics of the transformation.

A conservative finite difference scheme for Eq. (33) can be written as

$$\frac{\tilde{Q}^{n+1}_{i,j}-\tilde{Q}^{n}_{i,j}}{\Delta\tau}+\frac{\hat{E}^{m}_{i+1/2,j}-\hat{E}^{m}_{i-1/2,j}}{\Delta\xi}+\frac{\hat{F}^{m}_{i,j+1/2}-\hat{F}^{m}_{i,j-1/2}}{\Delta\eta}=0 \tag{35}$$

where $\hat{E}^{m}_{i+1/2,j}$ and $\hat{F}^{m}_{i,j+1/2}$ are numerical fluxes consistent with the transformed fluxes $\tilde{E}$ and $\tilde{F}$, respectively. As in the one-dimensional case, the difference scheme [Eq. (35)] is explicit when $m=n$ and implicit when $m=n+1$.

The numerical flux $\hat{E}_{i+1/2,j}$ for the first-order-accurate Osher scheme is given by

$$\hat{E}_{i+1/2,j}=\frac{1}{2}\left[\tilde{E}(Q_{i,j},\xi_{i+1/2,j})+\tilde{E}(Q_{i+1,j},\xi_{i+1/2,j})\right.$$
$$\left.-\int_{Q_{i,j}}^{Q_{i+1,j}}\left|\frac{\partial E}{\partial Q}(Q,\xi_{i+1/2,j})\right|\mathrm{d}Q\right] \tag{36}$$

The numerical flux $\hat{F}_{i,j+1/2}$ can be obtained from Eq. (36) by replacing $\tilde{E}$ and $\xi_{i+1/2,j}$ with $\tilde{F}$ and $\eta_{i,j+1/2}$, respectively. The evaluation of the integral in Eq. (36) is very similar to the procedure adopted in the one-dimensional case. Further details of the scheme in two dimensions can be found in Refs. 1 and 2.

By linearizing the numerical fluxes $\hat{E}^{n+1}_{i+1/2,j}$ and $\hat{F}^{n+1}_{i,j+1/2}$ with respect to the time-like variable τ and making approximations of the type in Eqs. (23-27), the implicit scheme in two spatial dimensions and in generalized coordinates becomes

$$\left[I+\frac{\Delta\tau}{\Delta\xi}(\Delta_\xi\tilde{A}^-+\nabla_\xi\tilde{A}^+)+\frac{\Delta\tau}{\Delta\eta}(\Delta_\eta\tilde{B}^-+\nabla_\eta\tilde{B}^+)\right]^n\Delta\tilde{Q}_{i,j}$$
$$=-\Delta\tau\left[\frac{\hat{E}^{n}_{i+1/2,j}-\hat{E}^{n}_{i-1/2,j}}{\Delta\xi}+\frac{\hat{F}^{n}_{i,j+1/2}-\hat{F}^{n}_{i,j-1/2}}{\Delta\eta}\right] \tag{37}$$

where

$$\tilde{A}^{\pm}=\left\{\frac{\partial\tilde{E}}{\partial\tilde{Q}}\right\}^{\pm}, \qquad \tilde{B}^{\pm}=\left\{\frac{\partial\tilde{F}}{\partial\tilde{Q}}\right\}^{\pm}$$

Similar to Eq. (28), the left-hand side of Eq. (37) corresponds to the split-flux scheme and the right-hand side (RHS) corresponds to the Osher scheme. However, a natural linearization of the Osher numerical flux, though impractical, can be obtained just as in the one-dimensional case. The final form for the proposed implicit Osher scheme [obtained by factoring Eq. (37)] is given by

$$\left[I+\frac{\Delta\tau}{\Delta\xi}(\Delta_\xi\tilde{A}^-+\nabla_\xi\tilde{A}^+)\right]\left[I+\frac{\Delta\tau}{\Delta\eta}(\Delta_\eta\tilde{B}^-+\nabla_\eta\tilde{B}^+)\right]\Delta\tilde{Q}_{i,j}$$
$$=\text{RHS of Eq. (37)} \tag{38}$$

A Spatially Second-Order-Accurate Version of the Scheme

The first-order-accurate schemes described above are insufficient to produce accurate results for a general class of problems. The explicit, second-order-accurate, total-variation-diminishing (TVD) version of the Osher scheme is developed in Ref. 2. The explicit scheme consists of a predictor-corrector sequence and is second-order accurate in both time and space. It employs flux limiters to achieve the TVD property. Further details of the scheme can be found in Ref. 2.

The implicit, spatially second-order-accurate scheme developed in this study takes the form

$$\left[I+\frac{\Delta\tau}{\Delta\xi}(\Delta_\xi\tilde{A}^-+\nabla_\xi\tilde{A}^+)\right]^n\left[I+\frac{\Delta\tau}{\Delta\eta}(\Delta_\eta\tilde{B}^-+\nabla_\eta\tilde{B}^+)\right]^n\Delta\tilde{Q}_{i,j}$$
$$=-\Delta\tau\left[\frac{\hat{E}^{n}_{i+1/2,j}-\hat{E}^{n}_{i-1/2,j}}{\Delta\xi}+\frac{\hat{F}^{n}_{i,j+1/2}-\hat{F}^{n}_{i,j-1/2}}{\Delta\eta}\right]$$
$$-\frac{\Delta\tau}{2\Delta\xi}[\Delta E^+(Q_{i+1,j},Q_{i,j},\xi_{i+1/2,j})$$
$$-\Delta E^+(Q_{i-2,j},Q_{i-1,j},\xi_{i-1/2,j})]^n$$
$$+\frac{\Delta\tau}{2\Delta\xi}[\Delta E^-(Q_{i+1,j},Q_{i+2,j},\xi_{i+1/2,j})$$
$$-\Delta E^-(Q_{i,j},Q_{i+1,j},\xi_{i-1/2,j})]^n$$
$$-\frac{\Delta\tau}{2\Delta\eta}[\Delta F^+(Q_{i,j-1},Q_{i,j},\eta_{i,j+1/2})$$
$$-\Delta F^+(Q_{i,j-2},Q_{i,j-1},\eta_{i,j-1/2})]^n$$
$$+\frac{\Delta\tau}{2\Delta\eta}[\Delta F^-(Q_{i,j+1},Q_{i,j+2},\eta_{i,j+1/2})$$
$$-\Delta F^-(Q_{i,j},Q_{i,j+1},\eta_{i,j-1/2})]^n \tag{39}$$

To obtain Eq. (39), the terms that contribute to second-order accuracy in space ($\Delta E^{\pm}$ and $\Delta F^{\pm}$) have been evaluated at the nth time level, and, hence, their time derivatives do not appear on the left-hand side of this equation. This results in block-tridiagonal matrices on the left-hand side of Eq. (39) instead of block-pentadiagonal matrices. In addition, approximations of the type made in Eqs. (23-27) have also been used in obtaining Eq. (39).

The implicit scheme given by Eq. (39) does not employ flux limiters and, in general, will result in spurious oscillations near captured discontinuities. It can be made to yield an almost oscillation-free solution at convergence (if the solution converges) by replacing $\Delta E^{\pm}$ and $\Delta F^{\pm}$ in Eq. (39) by the modified values $\Delta\bar{E}^{\pm}$ and $\Delta\bar{F}^{\pm}$, respectively. The modified fluxes are obtained as follows (the procedure is similar to the one used for the explicit scheme in Ref. 2); an entropy function $V(Q)$ is defined as

$$V(Q)=-\rho\log(p/\rho^\gamma) \tag{40}$$

The gradient of the entropy function with respect to the dependent variables is given by

$$V_Q = \nabla_Q V = \frac{-(\gamma-1)}{p}\left[e + \frac{p}{\gamma-1}\left(-\gamma - 1 + \log\frac{p}{\rho^\gamma}\right),\right.$$
$$\left. -\rho u,\ -\rho v,\ \rho\right]^T \tag{41}$$

The modification of the fluxes is done one subpath at a time. Defining $DV_Q^{(m)}$ (the change in V_Q along the subpath m) as

$$DV_Q^{(m)} = (V_Q)_{i+m/3,j} - (V_Q)_{i+(m-1)/3,j}, \quad m = 1,2,3 \tag{42}$$

the modified fluxes $(\overline{\Delta E^+})^{(m)}$ and $(\overline{\Delta E^-})^{(m)}$ along this subpath are evaluated from

$$[\overline{\Delta E^+}(Q_{i-1,j}, Q_{i,j}, \xi)]^{(m)} = [\Delta E^+(Q_{i,j}, Q_{i+1,j}, \xi)]^{(m)}$$
$$\times \max[0, \min(\phi, N/D)] \tag{43}$$

where

$$1.0 \le \phi \le 2.0$$

$$N = \langle [\Delta E^+(Q_{i-1,j}, Q_{i,j}, \xi)]^{(m)}, [DV_Q(Q_{i,j}, Q_{i+1,j}, \xi)]^{(m)} \rangle$$
$$D = \langle [\Delta E^+(Q_{i,j}, Q_{i+1,j}, \xi)]^{(m)}, [DV_Q(Q_{i,j}, Q_{i+1,j}, \xi)]^{(m)} \rangle$$

and (44)

$$[\overline{\Delta E^-}(Q_{i,j}, Q_{i+1,j}, \xi)]^{(m)} = [\Delta E^-(Q_{i-1,j}, Q_{i,j}, \xi)]^{(m)}$$
$$\times \max[0, \min(\phi, N/D)] \tag{45}$$

where

$$1.0 \le \phi \le 2.0$$

$$N = \langle [\Delta E^-(Q_{i,j}, Q_{i+1,j}, \xi)]^{(m)}, [DV_Q(Q_{i-1,j}, Q_{i,j}, \xi)]^{(m)} \rangle$$
$$D = \langle [\Delta E^-(Q_{i-1,j}, Q_{i,j}, \xi)]^{(m)}, [DV_Q(Q_{i-1,j}, Q_{i,j}, \xi)]^{(m)} \rangle$$

(46)

The symbols $\langle\ \rangle$ in Eqs. (44) and (46) represent the inner product of the two vectors contained within them. The modified values of $\Delta F^{\pm}$ are obtained in a similar manner.

A Newton-Iterative Approach to Solving the Nonlinear Equations

Equation (28) is a linearized form of the nonlinear implicit finite difference equations presented in Eq. (4) ($m = n+1$). The solution of Eq. (28) only approximates the solution of Eq. (4). The discrepancy between the two solutions can be large when the time rate of change of the solution is large (such as a shock moving rapidly through the grid or during an initial transient) or when the integration step size is large. Some of the desirable properties of the nonlinear equations, such as the monotonicity property that Eq. (4) possesses both in the explicit and implicit modes, may be lost upon linearization. The monotonicity of the solution is restored only when the solution converges to a time-asymptotic limit. However, the numerical oscillations obtained in the vicinity of discontinuities (in the transient stages) as a result of solving the linearized equations may become large enough to terminate the calculation (because of nonphysical solutions such as negative density) at large CFL numbers. Hence, it is advantageous to be able to solve the nonlinear equations at each time step. This can be done by adopting a Newton-iterative technique. The equation set that results upon performing a Newton linearization of Eq. (4) (with $m = n+1$) takes the form

$$\left[I + \frac{\Delta t}{\Delta x}[\Delta_x (A^-)^p + \nabla_x (A^+)^p]\right][Q^{p+1} - Q^p]$$
$$= -\left[Q^p - Q^n + \frac{\Delta t}{\Delta x}(\hat{E}^p_{i+1/2} - \hat{E}^p_{i-1/2})\right] \tag{47}$$

where p denotes the iteration number and Q^p is an iterative update of Q^{n+1}. When $p = 0$, $Q^p = Q^n$ and, when Eq. (47) converges, $Q^p = Q^{n+1}$. It is of interest that the left-hand side of Eq. (47) becomes zero at convergence for every integration step. This implies that Eq. (4), with $m = n+1$ [which corresponds to the right-hand side of Eq. (47)], is satisfied at each integration step. Hence, the monotonicity property is restored with the help of an iterative loop at each time step. A second point of interest is that the iterative scheme reverts to the noniterative scheme [Eq. (28)] when only one iteration is performed.

The second-order-accurate counterpart of Eq. (47) in two spatial dimensions is given by

$$\left[I + \frac{\Delta\tau}{\Delta\xi}[\Delta_\xi (\tilde{A}^-)^p + \nabla_\xi (\tilde{A}^+)^p]\right]$$
$$\times \left[I + \frac{\Delta\tau}{\Delta\eta}[\Delta_\eta (\tilde{B}^-)^p + \nabla_\eta (\tilde{B}^+)^p]\right][\tilde{Q}^{p+1}_{i,j} - \tilde{Q}^p_{i,j}]$$
$$= -\Delta\tau\left[\frac{\tilde{Q}^p_{i,j} - \tilde{Q}^n_{i,j}}{\Delta\tau} + \frac{\hat{E}^p_{i+1/2,j} - \hat{E}^p_{i-1/2,j}}{\Delta\xi}\right.$$
$$\left. + \frac{\hat{F}^p_{i,j+1/2} - \hat{F}^p_{i,j-1/2}}{\Delta\eta}\right]$$
$$- \frac{\Delta\tau}{2\Delta\xi}[\overline{\Delta E^+}(Q_{i-1,j}, Q_{i,j}, \xi_{i+1/2,j})$$
$$- \overline{\Delta E^+}(Q_{i-2,j}, Q_{i-1,j}, \xi_{i-1/2,j})]^p$$
$$+ \frac{\Delta\tau}{2\Delta\xi}[\overline{\Delta E^-}(Q_{i+1,j}, Q_{i+2,j}, \xi_{i+1/2,j})$$
$$- \overline{\Delta E^-}(Q_{i,j}, Q_{i+1,j}, \xi_{i-1/2,j})]^p$$
$$- \frac{\Delta\tau}{2\Delta\eta}[\overline{\Delta F^+}(Q_{i,j-1}, Q_{i,j}, \eta_{i,j+1/2})$$
$$- \overline{\Delta F^+}(Q_{i,j-2}, Q_{i,j-1}, \eta_{i,j-1/2})]^p$$
$$+ \frac{\Delta\tau}{2\Delta\eta}[\overline{\Delta F^-}(Q_{i,j+1}, Q_{i,j+2}, \eta_{i,j+1/2})$$
$$- \overline{\Delta F^-}(Q_{i,j}, Q_{i,j+1}, \eta_{i,j-1/2})]^p \tag{48}$$

In two dimensions, the iterative approach has the added advantage that the factorization error is driven to zero at each step, if the iteration converges. It has also been found that the iterative approach enhances stability; that is, it is possible to use larger CFL numbers than with noniterative schemes. It should be noted that, although the iterative approach permits the use of larger CFL numbers, there still exists a CFL limitation because at very large CFL numbers the iteration cycle may not converge due to factorization error. This problem can be overcome by resorting to relaxation methods that do not require factorization.[7] The primary disadvantage of the iterative approach is the added computation that the iterations require. This is offset to some extent by the larger step sizes that are possible with the iterative scheme. A second, but less limiting, factor is the increased storage requirement (one extra level to store Q^n).

Conservative Property of the Implicit Schemes Developed in this Study

Consider the finite difference form of the one-dimensional Euler equations given in Eq. (4):

$$\frac{Q_i^{n+1}-Q_i^n}{\Delta t}+\frac{\hat{E}^m_{i+1/2}-\hat{E}^m_{i-1/2}}{\Delta x}=0 \tag{49}$$

where $\hat{E}^m_{i+1/2}$ is the numerical flux consistent with the physical flux E. The numerical fluxes "telescope"; i.e., given a set of consecutive grid points $r...s$, the sum

$$S=\sum_{k=r}^{s}\frac{\Delta x}{\Delta t}[Q_k^{n+1}-Q_k^n]=-\sum_{k=r}^{s}[\hat{E}^m_{k+1/2}-\hat{E}^m_{k-1/2}]$$

reduces to

$$S=\hat{E}^m_{r-1/2}-\hat{E}^m_{s+1/2} \tag{50}$$

Equation (50) is a statement of global conservation of flux, since no residual fluxes (corresponding to points in the interior of the region $r...s$) are generated in the summation process, and Eq. (49) is a statement of local conservation of flux. Therefore, an integration scheme that can be expressed as in Eq. (49) with the help of numerical fluxes is conservative.

Both the explicit [$m=n$ in Eq. (49)] and nonlinear implicit schemes [$m=n+1$ in Eq. (49)] are, from the above discussion, conservative. The linearized implicit form given in Eq. (28) can also be shown to be conservative by defining a modified numerical flux as follows:

$$\bar{E}_{i+1/2}=\hat{E}^n_{i+1/2}+(A^-_{i+1})^n\Delta Q_{i+1}+(A^+_i)^n\Delta Q_i \tag{51}$$

Equation (28) can now be written as

$$\frac{Q_i^{n+1}-Q_i^n}{\Delta t}+\frac{\bar{E}_{i+1/2}-\bar{E}_{i-1/2}}{\Delta x}=0 \tag{52}$$

The conservative nature of Eq. (28) is now apparent. An identical procedure can be used to demonstrate that Eqs. (38) and (39) are also conservative in nature in their unfactored forms.

Earlier it was required that the numerical flux $\hat{E}^m_{i+1/2}$ be consistent with the physical flux E. The numerical flux for the explicit, fully implicit, and linearized implicit schemes can all be written in the form

$$\hat{E}_{i+1/2}=\hat{E}_{i+1/2}[Q_i,Q_{i+1},\Delta Q_i,\Delta Q_{i+1}] \tag{53}$$

Consistency implies that

$$\hat{E}[Q,Q,0,0]=E(Q) \tag{54}$$

Results and Discussion

Results are presented in this section for inviscid problems in one and two dimensions. The test cases include quasi-one-dimensional nozzle flow and supersonic flow past a cylinder. First-order-accurate results are presented for the nozzle and second-order-accurate results are presented for the cylinder problem.

Quasi-One-Dimensional Nozzle Flow

The first problem consisted of quasi-one-dimensional flow through a diverging nozzle. The area variation of the nozzle is given by

$$A(x)=1+x^2/2, \qquad 0\le x\le 1$$

The inlet conditions were supersonic ($M_i=2$) and the exit pressure was specified so that a shock occurred at $x=0.5$. A linear variation of the dependent variables between the inlet and exit conditions was assumed for the initial conditions. The equations of motion were then integrated to convergence using both the implicit scheme given by Eq. (28) (scheme A) and the implicit scheme that uses the "true" linearization of the Osher numerical fluxes, as in Eq. (22) (scheme B). The calculation was performed on an equispaced grid. The boundary conditions used at the two ends of the nozzle are also implicit in nature; see Ref. 8.

The integration was performed at a constant Δt of 0.187 (which corresponds to a CFL number ν between 14.0 and 15.0). Figure 2 shows the variation of the density as a function of the axial distance along the nozzle after 20 integration steps, obtained with schemes A and B. Clearly the transient solutions obtained with the two schemes are very nearly the same. Apparently, the approximations made in linearizing the numerical flux [Eqs. (23)] have a negligible effect on the time-accuracy of the solution for the case considered. One might suspect that any discrepancy between the two transients would increase with increasing Δt, since it is in the time linearization that the two methods differ. Clearly, such a discrepancy has not surfaced even at CFL numbers of approximately 14.5. It can also be seen that the transient solutions obtained at large values of ν are not monotonic (Fig. 2) in spite of the first-order accuracy of the method. However, the oscillations in the density profile are small.

Figure 3 shows the density profile obtained at convergence. The convergence criterion chosen was

$$|\Delta\rho_i|_{\max}<5\times10^{-4}$$

The implicit calculations were made at a CFL number of 15.0 and the explicit calculation at a CFL number of 0.99.

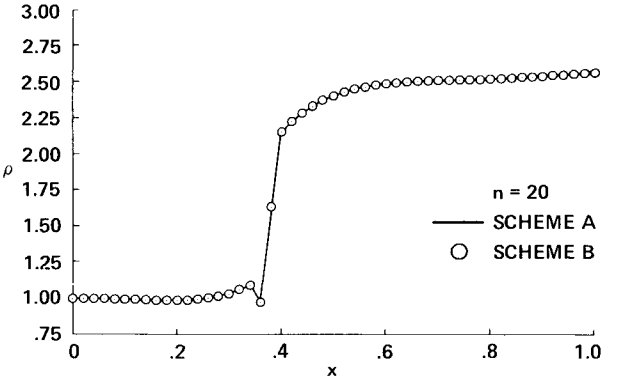

Fig. 2 Density distribution along the length of the nozzle after 20 integration steps.

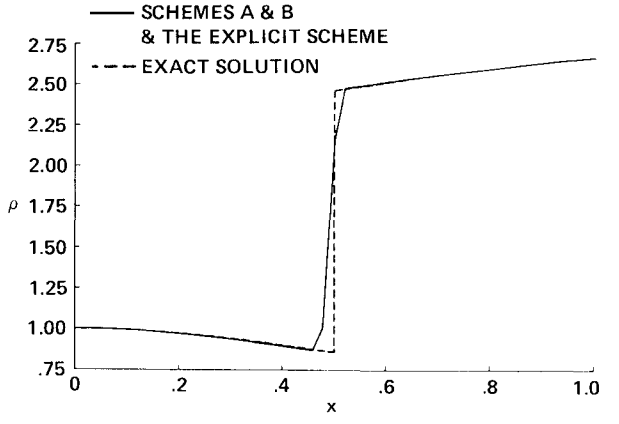

Fig. 3 Density distribution along the length of the nozzle at convergence.

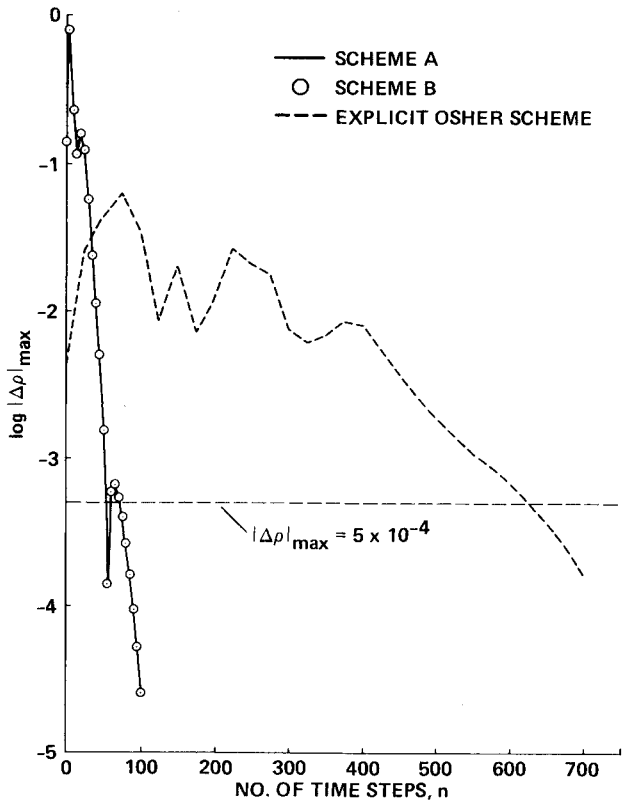

Fig. 4 Convergence history for the nozzle calculation (implicit and explicit calculations).

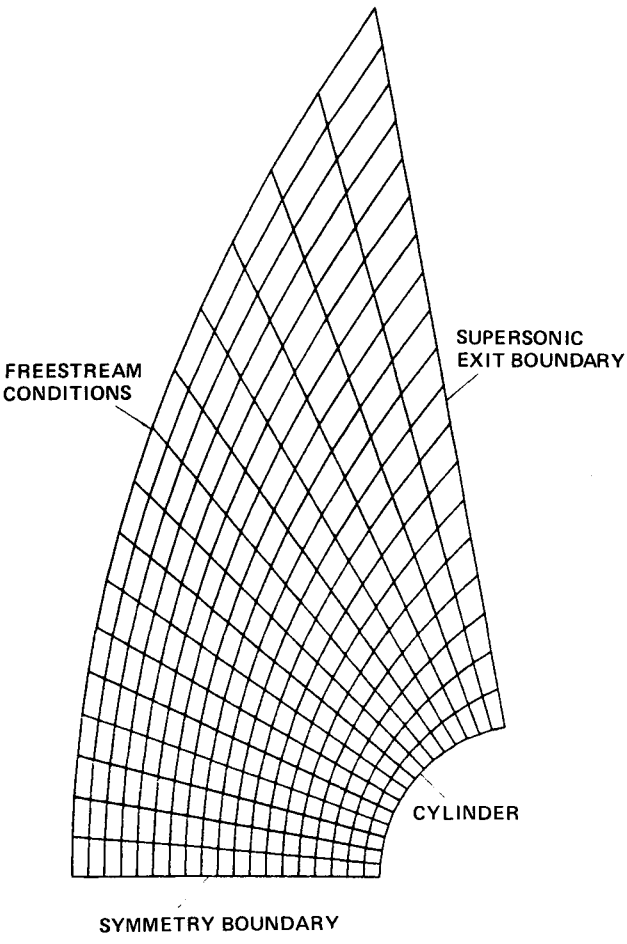

Fig. 5 Grid used for the cylinder calculation.

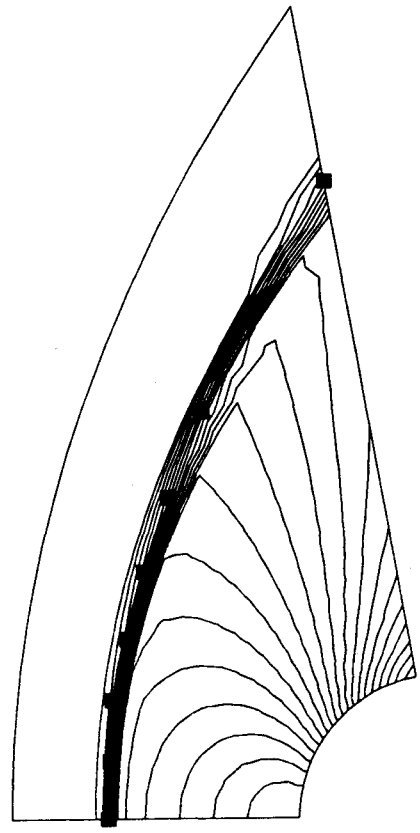

Fig. 6 Isobars obtained at convergence for the cylinder (second-order-accurate scheme).

All of the schemes yield identical converged results, as should be expected. The shock is sharp as guaranteed by the first-order-accurate Osher scheme and occurs over three mesh intervals. Figure 4 shows the convergence history for the explicit Osher scheme and schemes A and B. The implicit schemes converge about 8.7 times faster than the explicit scheme. However, scheme A required three times as much computing time as the explicit scheme per integration step and, hence, the actual computing cost is reduced by a factor of 2.9. Scheme B, on the other hand, requires four times as much computing time as the explicit scheme per integration step.

Time steps corresponding to CFL numbers greater than 16 resulted in unstable calculations with both schemes A and B. This instability is due to the invalidity of the time-linearization procedure in the presence of rapidly moving discontinuities (the linear initial profile in the preceding example develops into a shock at $x=0.3$ and the shock then moves to its steady-state position at $x=0.5$).

Cylinder in a Supersonic Freestream

To determine the acceleration in the convergence rate that can be obtained with the implicit scheme in two-dimensional problems, the flow associated with a cylinder in a supersonic freestream ($M=2$) was calculated. The grid used for the calculation is shown in Fig. 5. The dependent variables at all of the grid points were initialized to their freestream values. The equations of motion were integrated using both the explicit and implicit Osher schemes until the solution converged to its steady-state value. The first-order-accurate scheme is insufficient to yield accurate results in all cases. In order to obtain reliable results for a wide range of problems, it is necessary to use the second-order-accurate version of the scheme. Hence, the cylinder calculation was performed with second-order-accurate fluxes that were modified using the flux-limiting techniques described earlier. Implicit boundary conditions of the type described in Ref. 9 were used at the cylinder surface for the implicit calculations. Figure 6 shows

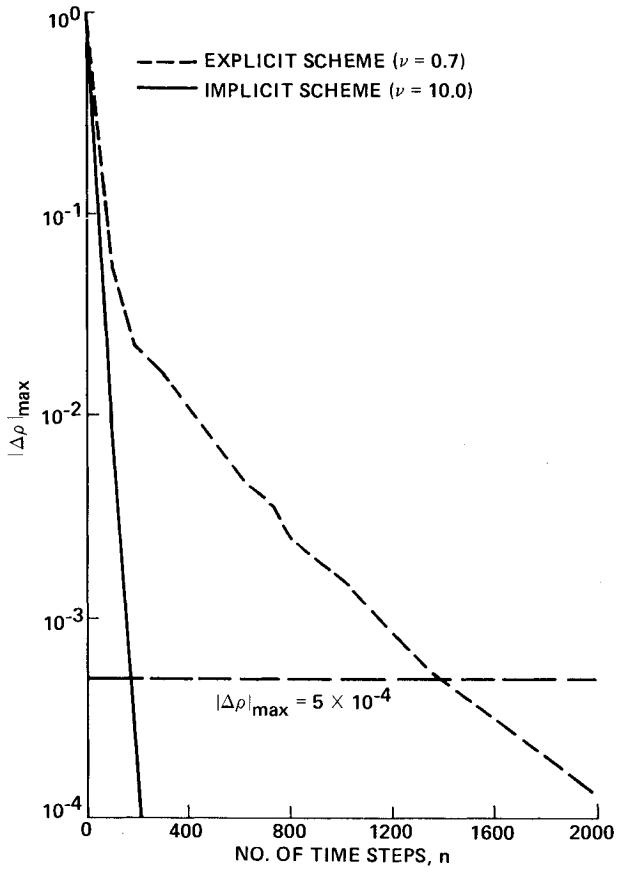

Fig. 7 Convergence history for the cylinder calculation (explicit and implicit second-order-accurate calculations).

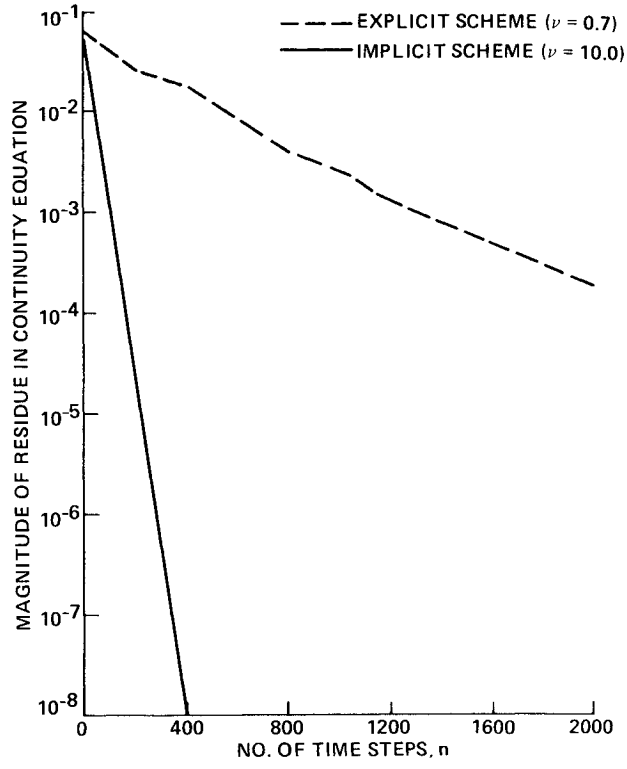

Fig. 8 Variation of residue in the continuity equation with integration step.

the pressure contours obtained at convergence with the second-order-accurate implicit scheme. The pressure contours obtained with both the implicit and explicit schemes were almost identical. The shock is seen to be almost oscillation-free. The square symbols in Fig. 6 represent the shock position predicted by another numerical approach.[10] The captured shock occurs directly on top of the predicted shock.

Figure 7 displays the convergence history for the explicit and implicit schemes. The convergence criterion chosen was

$$|\Delta\rho_{i,j}|_{\max} < 5 \times 10^{-4}$$

The explicit scheme took 1400 steps to converge, whereas the implicit scheme took only 177 steps. Thus the use of the implicit scheme increased the overall convergence rate by a factor of 7.9. Both the explicit and implicit codes were fully vectorized for use on the CRAY-XMP machine. The explicit and implicit calculations required 2.86 and 3.77 s of computing time per 100 steps, respectively. Since the implicit scheme requires approximately 1.32 times as much computing time as the explicit scheme per integration step, the computing cost is decreased by a factor of 6 using the implicit scheme. A CFL number of 0.70 was used for the explicit scheme (the maximum allowable CFL number being approximately 0.71). The implicit calculation was performed at a CFL number of 10.0. Time steps corresponding to CFL numbers larger than 10.0 resulted in longer convergence times for the implicit code, and eventually at a CFL number of 25.0 the code exhibited unstable behavior. Both the decreased stability limit and the existence of a rather small optimal CFL number are probably because of the explicit treatment of the terms that contribute to second-order spatial accuracy, i.e., inaccurate linearization, and also factorization error. Figure 8 shows the variation of the magnitude of the maximum residue R in the continuity equation as a function of the number of integration steps

$$R = [\text{RHS of Eq. (39)}]/\Delta\tau$$

The implicit scheme reduces R by seven orders of magnitude in 400 steps. Both curves are almost linear and the ratio of the average slopes is approximately 13.5 (implicit to explicit).

It should be kept in mind that calculations on almost equispaced grids, such as the one used in this calculation, are severe tests cases for studying the improvement in convergence rates that can be obtained with implicit schemes. The full potential of an implicit scheme can be realized only on a grid in which the mesh spacing varies widely.

As in the one-dimensional case, oscillatory behavior of the dependent variables in the vicinity of the shock was observed at large CFL numbers with the implicit scheme (in the transient stages). Both the factorization and linearization errors and the oscillatory behavior of transient solutions obtained with the implicit schemes developed in this study can be eliminated by using a Newton-iterative approach that solves the nonlinear implicit equations at each step. Figure 9 compares pressure distributions in a direction normal to the body surface (obtained after 25 integration steps). The pressure distributions are plotted along the symmetry line and a radial line inclined at 45 deg to the symmetry line. A comparison is made between the results obtained from the noniterative and iterative schemes. The initialization and boundary procedures used for the iterative scheme were the same as in the previous case. Five iterations were required at each time step to decrease the maximum residual by at least one order of magnitude at all of the grid points. The two pressure variations of Fig. 9 can be directly compared since they occur at approximately the same time. The absence of oscillations in the iterative calculation is clearly seen. The converged solution was, as expected, identical to the one obtained with the noniterative scheme.

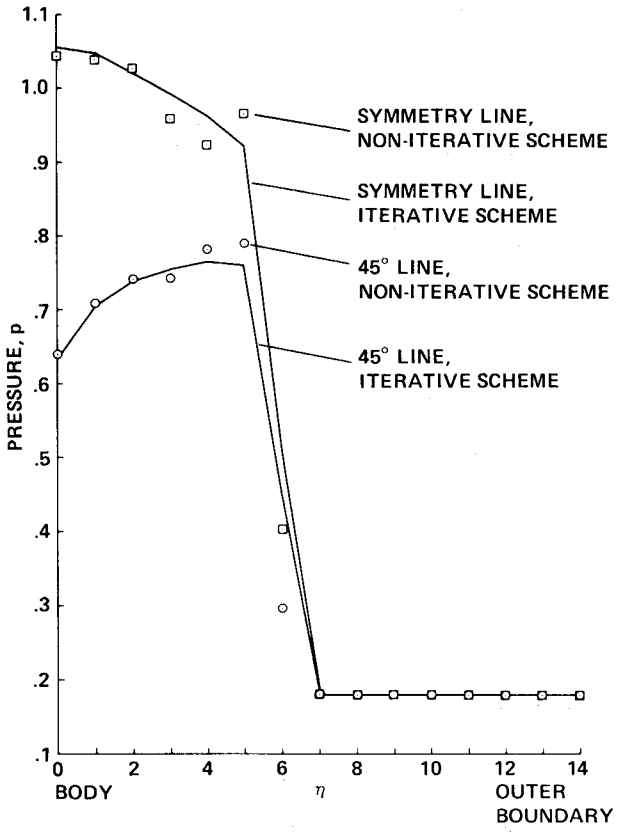

Fig. 9 Comparison of transient pressure distributions obtained with the iterative and noniterative schemes.

The principal disadvantage of the iterative scheme is the excessive computing time required per integration step because of the iterative nature of the scheme. However, the larger step sizes that are possible with the iterative scheme offset the additional computing cost (due to the iterations) to some extent. For example, at a CFL number of 15.0 and with two iterations per step, the iterative scheme converged in 155 steps. A detailed study of the iterative approach and the computer costs incurred in such calculations will be included in a future article.

Conclusions

The Osher scheme is a conservative, upwind, finite difference scheme. It has been found to be robust, with an excellent shock-capturing capability, and, because of the upwind differencing that it uses, models the physics of the problem correctly. However, in its explicit form it is restricted to CFL numbers less than 1.0 in one-dimensional problems and less than 0.71 in two-dimensional problems. In addition, the scheme requires many more arithmetic operations per integration step than simple central-difference schemes. Hence, it is computationally expensive to use.

Implicit forms for the first-order- and second-order-accurate Osher schemes are presented in this study. The equations are developed for the unsteady Euler equations in one and two dimensions (and in generalized coordinates for the two-dimensional case). Extending the scheme to three spatial dimensions is straightforward. The implicit schemes permit the use of larger CFL numbers (relative to explicit schemes) and thus accelerate convergence rates. Test cases used to demonstrate improvement in convergence rates include inviscid, quasi-one-dimensional nozzle flow and inviscid supersonic flow over a cylinder. The use of the implicit schemes accelerated convergence rates by almost an order of magnitude in most cases and resulted in considerable reductions in computing costs, thus justifying the development of the implicit forms.

To make the system of nonlinear implicit equations solvable in a noniterative fashion it is necessary to linearize the system of equations. Some of the desirable properties of the nonlinear system, such as monotonicity or the total variation-diminishing property, may be lost upon linearization. A Newton-iterative scheme that permits the solution of the nonlinear equations at each time step is developed in this study. A calculation demonstrating the restoration of the nonoscillatory behavior of the solution with the use of the iterative scheme is included. The iterative scheme has the added advantage that the factorization error is reduced to zero at every time step.

References

[1]Chakravarthy, S. R. and Osher, S., "Numerical Experiments with the Osher Upwind Scheme for the Euler Equations," *AIAA Journal*, Vol. 21, Sept. 1983, pp. 1241-1248.

[2]Chakravarthy, S. R. and Osher, S., "High Resolution Applications of the Osher Upwind Scheme for the Euler Equations," AIAA Paper 83-1943, 1983.

[3]Rai, M. M., Hessenius, K. A., and Chakravarthy, S. R., "Metric-Discontinuous Zonal Grid Calculations Using the Osher Scheme," *Computers & Fluids*, Vol. 12, No. 3, 1984, pp. 161-175.

[4]Chakravarthy, S. R., "Applications of the Osher Upwind Scheme to the Gas Dynamic Equations," Final Report for NASA Grant NAG1-269, Department of Aeronautics and Astronautics, Stanford University, Stanford, CA, July 1983.

[5]Steger, J. L. and Warming, R. F., "Flux Vector Splitting of the Inviscid Gas Dynamics Equations with Application to Finite Difference Methods," *Journal of Computational Physics*, Vol. 40, April 1981, pp. 263-293.

[6]Jespersen, D. C. and Pulliam, T. H., "Flux Vector Splitting and Approximate Newton Methods," AIAA Paper 83-1899, 1983.

[7]Chakravarthy, S. R., "Implicit Upwind Schemes with Approximate Factorization," AIAA Paper 84-0165, 1984.

[8]Chakravarthy, S. R., "Euler Equations—Implicit Schemes and Boundary Conditions," *AIAA Journal*, Vol. 21, May 1983, pp. 699-706.

[9]Rai, M. M. and Chaussee, D. S., "New Implicit Boundary Procedures: Theory and Application," *AIAA Journal*, Vol. 22, Aug. 1984, pp. 1094-1100.

[10]Lyubimov, A. N. and Rusanov, V. V., "Gas Flows Past Blunt Bodies," NASA TT-F 715, 1973.